

# Defects and multistability in eutectic solidification patterns

ANDREA PARISI<sup>1,2</sup> and MATHIS PLAPP<sup>1</sup>

<sup>1</sup> *Physique de la Matière Condensée, École Polytechnique, CNRS, 91128 Palaiseau, France*

<sup>2</sup> *Centro de Física da Matéria Condensada and Departamento de Física, Faculdade de Ciências, Universidade de Lisboa, Av. Prof. Gama Pinto 2, 1649-003 Lisboa Codex, Portugal*

PACS 64.70.kd – Metals and alloys

PACS 81.30.Fb – Solidification

PACS 05.70.Ln – Nonequilibrium and irreversible thermodynamics

**Abstract.** - We use three-dimensional phase-field simulations to investigate the dynamics of the two-phase composite patterns formed upon during solidification of eutectic alloys. Besides the spatially periodic lamellar and rod patterns that have been widely studied, we find that there is a large number of additional steady-state patterns which exhibit stable defects. The defect density can be so high that the pattern is completely disordered, and that the distinction between lamellar and rod patterns is blurred. As a consequence, the transition from lamellae to rods is not sharp, but extends over a finite range of compositions and exhibits strong hysteresis. Our findings are in good agreement with experiments.

The spontaneous emergence of solidification microstructures during the freezing of pure substances and alloys is a classic example for pattern formation outside of equilibrium. These structures are of considerable practical importance in metallurgy because of their influence on the properties of the finished material [1]. Solidification experiments also provide a particularly well-controlled setting to study fundamental questions of nonlinear pattern dynamics [2].

Eutectic alloys exhibit a triple point in their phase diagram at a temperature  $T_E$ , where liquid of composition  $C_E$  can coexist with two solid phases  $\alpha$  and  $\beta$  of different compositions  $C_\alpha$  and  $C_\beta$ . Growth from a liquid of composition sufficiently close to  $C_E$  leads to the formation of a composite solid, with two basic growth morphologies: alternating parallel platelets (lamellae) of the two solid phases, or fibres (rods) of one phase inside a matrix of the other, with the centres of the fibres located on a triangular lattice. In cross-sections of the finished material, the two morphologies look like stripes and round dots, respectively. This is reminiscent of the stripe and hexagon patterns that appear in many two-dimensional or quasi-two-dimensional systems, both out of equilibrium (e. g. Turing patterns, convection, reaction-diffusion systems) and in equilibrium (e. g. thin magnetic films, block copolymers). This is of course not accidental: like in these systems, two antagonistic effects (here, solute redistribution by diffusion and surface tension) lead to the emergence of a characteristic

length scale.

While it has been known for a long time that rods are preferred over lamellae when the volume fraction of one of the two phases is small, the precise conditions for the appearance of these two morphologies, as well as the nature of the transition between them, have remained unclear. Here, we show by quantitative three-dimensional phase-field simulations of eutectic solidification that the transition from rods to lamellae has some features that are not observed in other systems. We observe that regular arrays of rods exhibit, when their spacing is increased, a bifurcation from circular rods to symmetry-broken rods that have an oval or even dumbbell-like shape. The resulting stable arrays look like broken lamellae. There is thus a whole family of spatially periodic states “in between” rods and lamellae. Furthermore, we find that besides these periodic states, a large number of disordered steady-state configurations exist which consist of a mixture of rods and lamellae. Whereas such disordered states have also been found in other systems, they seem to be particularly stable in eutectic solidification. As a consequence of the existence of these numerous intermediate stable states, the transition from rods to lamellae is strongly hysteretic. All of these observations compare favourably to recent experimental findings.

Let us start out by a brief review of what is known on the two types of periodic patterns in eutectics. We consider directional solidification: a sample is pulled with fixed ve-

locity  $V$  in an externally imposed temperature gradient  $G$ . The liquid freezes into two distinct solid phases of different compositions. If all crystallographic effects are neglected and the isotherms are assumed to be planar, the problem is invariant by rotations and translations in the plane of the isotherms. Under these conditions, Jackson and Hunt [3] obtained two families of approximate steady-state solutions for perfectly periodic lamellae and rods, and related the average front temperature to the lamella or rod spacing  $\lambda$ . This front temperature is determined by the interplay between the diffusive redistribution of alloy components through the liquid and the effect of surface tension, which shifts the interface temperature by an amount that is proportional to the local interface curvature. For the slow growth regime that is relevant for most experiments (small Péclet number,  $\lambda V/D \ll 1$ , where  $D$  is the solute diffusion coefficient in the liquid), the global front undercooling with respect to the eutectic temperature is minimal for a characteristic spacing  $\lambda_{JH} = KV^{-1/2}$ , where the constant  $K$  depends on the thermophysical properties of the alloy, the volume fractions of the phases, and the type of pattern (lamellae or rods).

In order to be observable in experiments, the steady-state solutions must be stable. Some possible instabilities were already discussed by Jackson and Hunt [3]. Subsequent research has shown both through experiments and simulations that stable lamellar growth occurs within a range of lamellar spacings around  $\lambda_{JH}$  both in thin [4–7] as well as in extended samples [8, 9]; for a more detailed review, see [10]. Much less is known about the stability of rods. Recent advances have been obtained by using samples of transparent organic alloys [11, 12]. Numerically, a few examples of rod structures have been calculated by phase-field models [13, 14], but to our knowledge no detailed quantitative investigation of the steady-state solutions was previously carried out. We therefore start our investigations by a detailed survey of rod stability.

We use an efficient phase-field model recently introduced to simulate coupled eutectic growth [15, 16], and used previously to investigate the nature of pattern instabilities of lamellar arrays in massive samples [8] as well as the influence of temperature profiles on the solidified patterns [17]. The model has proved to be capable of producing results in excellent agreement with experimental observations [8, 16, 17]. The equations of the model as well as the method to choose appropriate computational parameters are discussed in detail in Refs. [8, 16]. The essential point is that in this model, the thickness  $W$  of the diffuse interfaces can be chosen freely without introducing computational artefacts as long as it remains about an order of magnitude smaller than the size of the smallest features in the pattern. Since we are interested here in general aspects of eutectic solidification, we use a eutectic alloy with a symmetric phase diagram, which yields the best computational performance. In this case, all relevant physical parameters can be grouped to yield three characteristic length scales: the thermal length  $l_T = |m|\Delta C/G$ ,

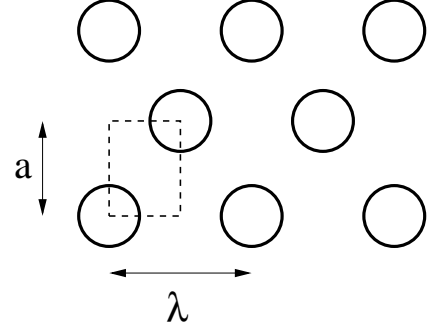


Fig. 1: Sketch of the simulation geometry. A perfectly periodic rod array of horizontal spacing  $\lambda$  and distance  $a$  between rows is simulated in the reduced simulation cell indicated by the dashed rectangle, with reflection boundary conditions.

the diffusion length  $l_D = D/V$ , and the capillary length  $\bar{d} = \gamma T_E / (L|m|\Delta C)$ , with  $m$  the liquidus slope,  $\Delta C$  the difference in composition between the two solids,  $\gamma$  the solid-liquid surface tension,  $T_E$  the eutectic temperature, and  $L$  the latent heat of melting. For all our simulations, we use  $l_D/d_0 = 10^3$  and  $l_T/l_D = 4$ .

The simulation setup is similar to the one used in Ref. [8]. A rectangular simulation cell is filled by the solid composite up to the solid-liquid interface, and by the liquid phase beyond it. The isotherms (and hence also the solid-liquid interface) advance at constant speed  $V$ , and the simulation cell is moved whenever the front has advanced by a certain amount, so that the interface is approximately stationary in the cell. An efficient multi-grid scheme permits to calculate the concentration field  $C(\vec{x}, t)$  up to a very large distance from the interface. An important parameter is the initial composition  $C_0$  of the liquid, because it determines the equilibrium volume fraction  $\eta$  of the  $\beta$  phase through the lever rule,  $\eta = (C_0 - C_\alpha)/\Delta C$ .

Since it turns out that distortions of the rod array play an important role for the interpretation of our results, it is useful to give some details about the geometry of our simulation cell, shown in Fig. 1. We consider perfectly periodic arrays of rods, where the distance between rods in a “horizontal” row (along the  $x$  direction) is  $\lambda$ , and the distance between rows is  $a$ . Steady states of such periodic rod arrays can be efficiently simulated by taking advantage of the two orthogonal planes of mirror symmetry that run through the center of each rod. We use the reduced simulation box indicated by a dashed rectangle, with reflection boundary conditions on all lateral boundaries for all fields. The simulation cell thus contains only two quarters of rods in two corners. The picture of a full array can be reconstructed by adding suitably reflected and shifted copies of the simulation cell. The simulation is initialised with two circular quarter-rods, where the radius is chosen such that the volume fractions of the two solid phases are consistent with the global alloy composition. The evolution of this initial state is then followed until a steady state is reached.

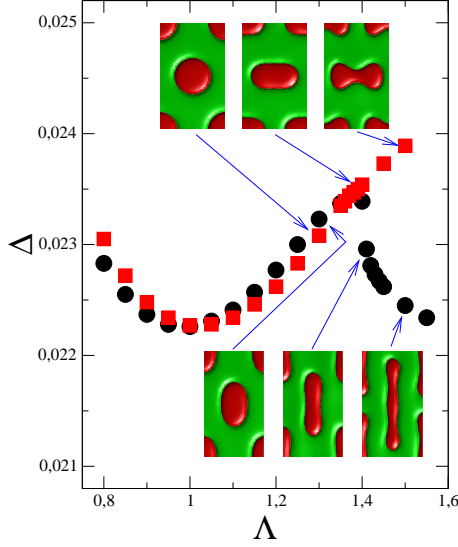


Fig. 2: Front undercooling  $\Delta$  versus reduced spacing  $\Lambda = \lambda/\lambda_{JH}$  for rod arrays of two different geometries and volume fraction of the  $\beta$  phase of  $\eta = 0.3$ . Circles:  $a/\lambda = 14/16$ ; squares:  $a/\lambda = 13/16$ . Insets: reconstructed steady states.

A perfect triangular lattice would correspond to  $a/\lambda = \sqrt{3}/2$ . However, since our finite-difference discretization uses a regular cubic grid, our simulation box has a rational aspect ratio, which results in a weakly distorted array. In such an array, the spacings between rods in a horizontal row and between rods in two distinct rows are slightly different. We will use the spacing  $\lambda$  within a horizontal row in our subsequent plots. To investigate various spacings at fixed aspect ratio, we keep the size of the simulation box in terms of grid points as well as the ratio of the grid spacing  $\Delta x$  and interface thickness  $W$  constant (we use  $\Delta x/W = 0.8$ ), whereas we vary the ratio  $W/\bar{d}$ , which corresponds to changing the physical size of the simulation box. Typically, we use 32 grid points along the smaller dimension of the box (of length equal to  $\lambda/2$ , see Fig. 1), which corresponds to a resolution of  $\lambda/W = 51.2$ , sufficient to guarantee well-converged results [8, 16].

We consider first the case of a sample with volume fraction  $\eta = 0.3$  of the  $\beta$  phase (for our symmetric phase diagram, the eutectic point is at  $\eta = 0.5$ ). In Fig. 2, we plot the dimensionless undercooling

$$\Delta = \frac{T_E - T_{\text{front}}}{|m|\Delta C}$$

as a function of the reduced spacing  $\Lambda = \lambda/\lambda_{JH}$ , where  $\lambda_{JH}$  is the minimum undercooling spacing calculated from the Jackson-Hunt theory for rods. Data for two different distorted arrays are shown. For an aspect ratio of  $a/\lambda = 14/16$ , which is slightly larger than  $\sqrt{3}/2$ , the undercooling curve exhibits a minimum at a spacing very close to the one predicted by the Jackson-Hunt calculation, and follows the expected behaviour  $\Delta = \Delta_{\min}(\Lambda + 1/\Lambda)$  [3] up to spacings of about  $\Lambda = 1.3$ . However, as the spac-

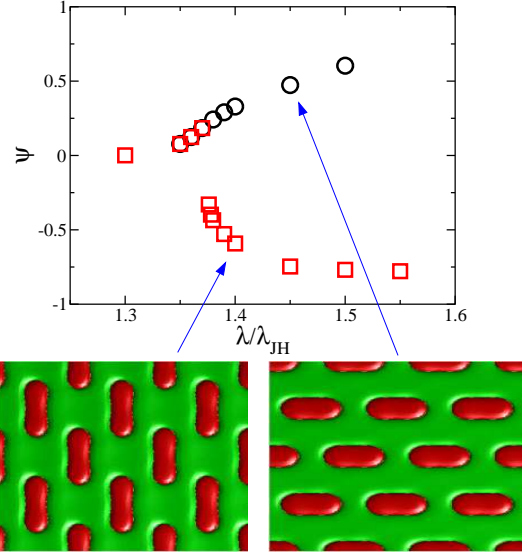


Fig. 3: Bifurcation diagram of the shape transition for  $a/\lambda = 13/16$  and  $\eta = 0.3$ . The parameter  $\psi$  is plotted versus the initial rod spacing. Squares and circles denote runs with different initial conditions: circles, cylindrical rods; squares, rods elongated towards second neighbours. The top and bottom branches correspond to rods with a cross-section elongated towards first and second neighbours, respectively, as shown in the pictures of reconstructed arrays (both for  $\Lambda = 1.4$ ). The centres of the elongated rods remain on the initial rod lattice.

ing increases, we observe a change in shape from circular rods to elongated rods with the long axis oriented towards the second nearest neighbours (see Fig. 3 for the view of a reconstructed array). At the same time, the undercooling starts to differ markedly from the Jackson-Hunt prediction. For a slightly lower aspect ratio of  $a/\lambda = 13/16$ , smaller than  $\sqrt{3}/2$ , the undercooling curve again exhibits a minimum for a slightly larger spacing, but upon increasing the spacing, this time the rods elongate in the direction of the *first* neighbours.

In fact, both of these elongated states can be reached for each aspect ratio by starting from initial conditions which favour one direction or the other, such as elliptic rods elongated towards the first or the second nearest neighbours instead of simple circular rods. Thus, the shape transition is a bifurcation. For a more quantitative description, we define a shape parameter

$$\psi = \frac{d_1 - d_2}{d_1 + d_2}$$

with  $d_1$  and  $d_2$  being the diameter of the rod along axes oriented towards the first and second nearest neighbours, respectively. A perfectly circular rod corresponds to  $\psi = 0$ , whilst for a deformation towards first (second) nearest-neighbours  $\psi$  has a positive (negative) sign. This parameter is plotted versus the spacing in Fig. 3 for  $a/\lambda = 13/16$ . Note that the bifurcation is asymmetric because stretching of the rods towards first and second nearest neighbours is not equivalent. Furthermore, for this

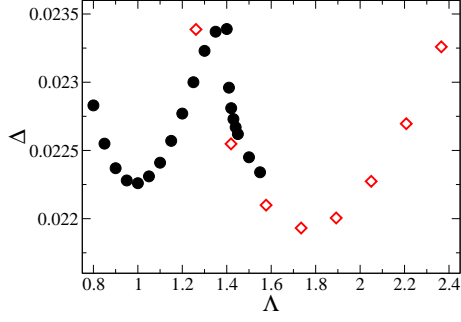


Fig. 4: Comparison of the front undercooling  $\Delta$  of rods with  $a/\lambda = 14/16$  (circles), and lamellae of half the original rod spacing (diamonds). In order to achieve a direct comparison of corresponding states, for the lamellae the reduced spacing was calculated as  $\Lambda = 2\lambda/\lambda_{JH}$ , where  $\lambda_{JH}$  is the rod minimum undercooling spacing.

aspect ratio, the single branch of weakly distorted rods that exists below the bifurcation threshold connects continuously to the upper branch of solutions (horizontally elongated rods), whereas the second branch appears by a discontinuous jump of the shape parameter. The opposite behaviour is observed in the bifurcation diagram for the aspect ratio  $a/\lambda = 14/16$  (not shown): here, the single branch exhibits slightly negative values of  $\psi$  when it approaches the bifurcation threshold, and connects continuously to the lower solution branch (vertically elongated rods). Thus, both elongated rod states are stable steady-state solutions, but their respective basins of attraction depend on the distortion of the initial rod array. Elongation is always favoured in the direction that is stretched with respect to a symmetric hexagonal array.

As can be appreciated from Fig. 3, the periodic arrays of elongated rods become similar, for both orientations, to a set of “broken” parallel lamellae, with a spacing  $\lambda_l = \lambda/2$  for the case of  $\psi < 0$  and  $\lambda_l = a$  for  $\psi > 0$ . Indeed, this is not just a geometrical similarity: in Fig. 4, it can be seen that the undercooling of a broken lamellar state with  $\psi < 0$  is very close to the one for perfect lamellae of half the original spacing. Note that we have plotted the curve for lamellae as a function of  $2\lambda$  in order to obtain a meaningful comparison in this graph. The shape change from circular rods to elongated rods takes place approximately at the intersection of the two Jackson-Hunt curves. This observation provides a simple criterion to predict the occurrence of the morphology transition, although it gives no direct explanation for the mechanism that is at work. Note that we have not observed any reconnection of the “broken lamellae” up to the largest spacings investigated ( $\Lambda = 1.55$ ).

The behaviour of the horizontal broken lamellae in the case  $a/\lambda = 13/16$  is quite different. The undercoolings for lamellae of spacing  $a$  are not very different from the original Jackson-Hunt curve for rods of spacing  $\lambda$ ; the undercoolings of the horizontal broken lamellae thus do not exhibit a dramatic change with the spacing. However,

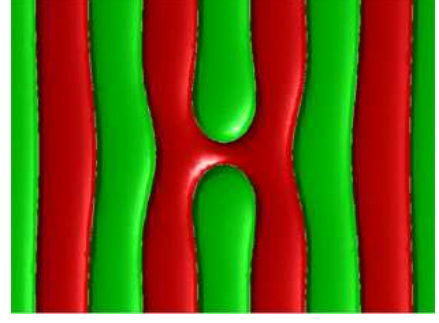


Fig. 5: Lamellar array with a single defect that remains stable. The snapshot shown is a steady state.

this branch of symmetry-broken solution terminates for  $\Lambda$  slightly above 1.5. The dumbbell-shaped rods shown in Fig. 2 split in two and reconnect to form vertical broken lamellae.

In summary, the “broken lamellae” or “elongated rod” states have properties that are very close to the ones of standard lamellae. Therefore, the morphological change can be interpreted as a transition to a lamellar array that is not completed, since neighbouring rods do not connect. Clearly, a barrier prevents the establishment of a simple lamellar pattern. Further simulations reveal that the existence of such barriers is a general property: whenever defects exist in a eutectic solidification pattern, they are very difficult to heal. A typical example is shown in Fig. 5. The initial condition for this simulation is an array of parallel lamellae, where a “cut” has been made in the central lamella, thus creating two lamella terminations facing each other. The pattern could come back to a perfect lamellar array by just reconnecting the two terminations; instead, after an initial transient where the two endings slightly adapt in shape and length, the simulation evolves towards the steady state shown in Fig. 5. It is thus clear that there exists a large number of steady states that exhibit stable defects. Indeed, by repeating the operation of “cutting” a lamella, an arbitrary number of defects can be introduced in a lamellar pattern. Inversely, if in a perfect rod pattern two rods are “connected” to form a piece of lamella, the latter persists as a stable steady state. It is even possible to create stable patterns which are a complete mix of lamellae and rods, such as shown in Fig. 6.

The presence of multiple steady states separated by “barriers” implies that a system started from random initial conditions will in general not reach a spatially periodic steady state. Fig. 7 shows examples of pattern evolution in an extended system using as initial condition a solid consisting of a random distribution of the two phases. For the eutectic composition, the emerging pattern is a complex network of lamellae, the evolution of which is very fast at first: reconnections between lamellae occur which lead towards a more ordered system. However, later on the evolution becomes very slow, since it is increasingly difficult for the system to overcome the barriers which



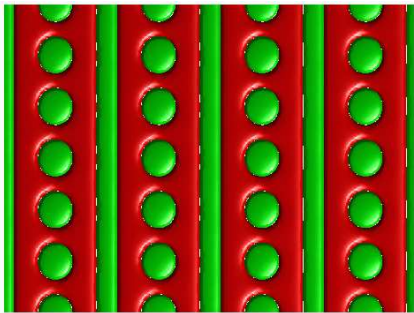


Fig. 6: Coexistence of rods and lamellae. The snapshot shown is a steady state.

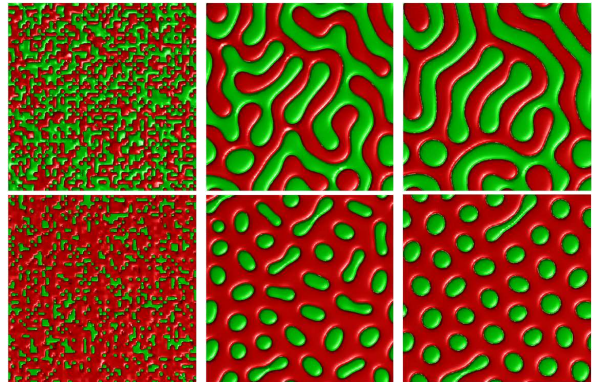


Fig. 7: (Colour online) Simulations of the symmetric model alloy at the eutectic composition ( $\eta = 0.5$ , top row) and at  $\eta = 0.3$  (bottom row) in an extended system. The initial state is a random distribution of patches of the two solid phases. We have used  $\bar{d}/W = 0.06218$ , and the lateral system size is  $160 W$ , which corresponds to  $1.6 l_D$  and  $6.5 \lambda_{JH}$  (at the eutectic composition). Snapshots for both simulations were taken at times  $t/t_D = 0, 0.90$  and  $21.87$ , where  $t_D = l_D^2/D$  is the diffusion time; the last frame reflects a total solidified length of  $127.39 \lambda_{JH}$ .

hinder reconnection. Interestingly, the resulting pattern shows, in addition to the emerging lamellar pattern, also a few isolated rods, which remain stable until the end of the simulation. For a  $\beta$  volume fraction of  $\eta = 0.3$ , mostly rods are formed that are disordered and elongated at first and then rearrange into a more ordered pattern. Note, however, that a few isolated “pieces of lamellae” remain. A series of similar simulations for various volume fractions shows that “pure” rod patterns are formed only for volume fractions below  $\eta \approx 0.25$ . It should be noted in passing that the final state for  $\eta = 0.3$  mostly consists of rods, although it can be seen from Fig. 4 that the global minimum undercooling is lower for lamellae at this composition. It is therefore clear that the criterion of lowest undercooling, often used in the metallurgical literature, is not sufficient to predict the emerging morphology.

These findings imply that the switching between lamellar and rod patterns which is observed in real samples can only be explained by the presence of a sufficiently large driving force. In fig. 8 we explore one possibility for such global forcing: a change of composition with time. The simulation is started from a state of highly unstable parallel lamellae, which rapidly break up and form the irregular pattern of rods shown in the first snapshot. The average concentration in the liquid far ahead of the growth front is changed linearly with time, which implies a change in volume fraction from  $\eta = 0.2$  to  $\eta = 0.8$  in the course of the simulation. The figure shows that a transition between rod and lamellar patterns can be triggered, but also shows that there is a strong hysteresis: the transition from rods to lamellae occurs at a volume fraction of  $\eta \approx 0.5$ , whilst the one from lamellae to rods occurs at  $\eta \approx 0.7$ . If the composition was decreased again starting from the last picture, the transition from rods to lamellae would happen again at  $\eta \approx 0.5$ , which shows that the patterns found for volume fractions between these two limits depend on the history of the system.

It is interesting to notice that both the lamellar and rod patterns that emerge after the transitions are clearly more regular than the ones obtained from random initial conditions. This is a result of a non-trivial spatial organisation of these transitions. The formation of lamellae occurs by

successive connections of rods, which could lead to a random lamellar pattern. However, as was discussed above, if the initial rod array is not perfectly hexagonal, but slightly distorted, the shape bifurcation favours a well-defined direction of elongation, which leads to the formation of large patches of parallel lamellae. The transition from lamellae to rods, in turn, starts at lamella terminations and propagates along lamellae by successive pinch-offs of new rods from the ending of the lamella; this leads then to the breakup of neighbouring lamellae. It would be highly interesting to study the dynamics of these transitions in more detail, but this is outside the scope of the present work.

All our results are in excellent agreement with experimental observations. Rods that are elongated (both towards first and second neighbours) have been observed in Al-Cu [18], mixed states of lamellae and rods have been found both in Al-Cu [19] and in transparent organic alloys [9]. In Fig. 7c of Ref. [20], alternating lamellae and rows of rods can be seen, which bear a striking similarity to our Fig. 6. Furthermore, it was shown that labyrinth states evolve indeed very slowly in time in the absence of external forcings [17]. Patterns of coexisting rods and lamellae were also observed in the peritectic Cu-Sn alloy [21].

Both aspects described above – shape instabilities of rods and disordered and “mixed” states – have been observed in other pattern-forming systems, but there are important differences between our findings and the ones reported in the literature. For instance, instabilities leading to dumbbell-shaped domains have been observed in ferrofluid droplets [22], and epitaxial islands [23], and have been analysed theoretically in systems with a Coulomb interaction [24]. However, in all these systems a long-range

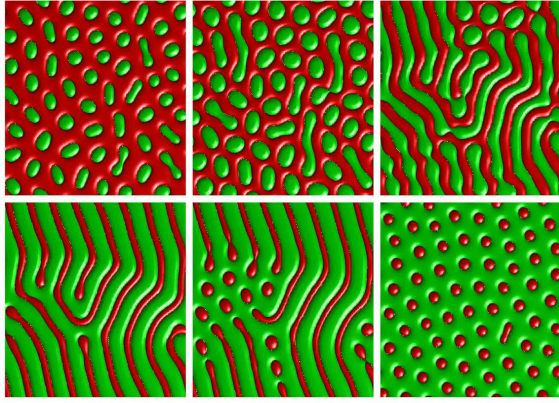


Fig. 8: (Colour online) Simulation of the symmetric model alloy in an extended system, where the volume fraction of  $\beta$  phase is varied from  $\eta = 0.2$  to  $\eta = 0.8$  over a time of  $19.2 t_D$ . Snapshots are taken at  $t/t_D = 3.2, 8.3, 10.2, 15.4, 16.7$ , and  $19.2$ ; the lateral system size is  $1.6 l_D$ , the same as in Fig. 7.

repulsion leads to the fact that the “tips” of the domains tend to avoid each other, instead of forming stripe-like assemblies like in our case. Furthermore, it is also well known that the transition from rods to lamellae is hysteretic; in thin magnetic films, this can be explicitly shown by a calculation of the energies associated with each pattern [25]. However, in most cases once the rods get unstable, they immediately connect to form lamellae, the only experimental evidence we are aware of for a (weakly) symmetry-broken spot pattern being Refs. [26,27]. Furthermore, coexistence between rods and lamellae was observed [28,29] but coexisting domains of stripes and rods are usually quite homogeneous, very distinct from the totally disordered and mixed patterns that we get.

Whereas it is difficult to pinpoint the exact origin of this difference between eutectic solidification and other pattern-forming systems, a few ideas can be advanced to motivate further investigation. First, whereas most of the systems mentioned above can be treated as quasi-two-dimensional, the eutectic growth front is three-dimensional. As mentioned above, one of the main effects that determine the front structure is capillarity. Clearly, defects in the pattern are surrounded by a specific local distribution of curvature, which can make the effective interaction between them more complicated than the standard attraction or repulsion generally expected for topological defects. Second, most of the patterns mentioned above arise when the system undergoes a bifurcation from a homogeneous to a patterned state (e.g. convection). In eutectic solidification, a homogeneous base state does not exist. Therefore, if the standard phenomenology of pattern formation applies at all, eutectic solidification most likely corresponds to a regime far beyond the bifurcation, where nonlinear effects are strong. Both of these points can yield potential explanations for the existence of barriers.

\*\*\*

We thank S. Akamatsu, S. Bottin-Rousseau, and G. Faivre for many discussions. This work was supported by the Centre National d’Etudes Spatiales (France).

## REFERENCES

- [1] DANTZIG J. A. and RAPPAPAZ M., *Solidification* (EPFL Press, Lausanne, Switzerland) 2009
- [2] CROSS M. C. and HOHENBERG P. C., *Rev. Mod. Phys.*, **65** 851 (1993)
- [3] JACKSON K. A. and HUNT J. D., *Trans. Metall. Soc. AIME*, **236** 1129 (1966)
- [4] KARMA A. and SARKISSIAN A., *Metall. Mat. Trans. A*, **27** 635 (1996)
- [5] GINIBRE M., AKAMATSU S. and FAIVRE G., *Phys. Rev. E*, **56** 780 (1997)
- [6] AKAMATSU S., PLAPP M., FAIVRE G. and KARMA A., *Phys. Rev. E*, **66** 030501(R) (2002)
- [7] AKAMATSU S., PLAPP M., FAIVRE G. and KARMA A., *Metall. Mat. Trans. A*, **35** 1815 (2004)
- [8] PARISI A. and PLAPP M., *Acta Mater.*, **56** 1348 (2008)
- [9] AKAMATSU S., BOTTIN-ROUSSEAU S. and FAIVRE G., *Phys. Rev. Lett.*, **93** 175701 (2004)
- [10] KARMA A. and PLAPP M., *JOM-US*, **56** 28 (2004)
- [11] SEREFOGLU M. and NAPOLITANO R. E., *Acta Mater.*, **56** 3862 (2008)
- [12] PERRUT M. ET AL., *Phys. Rev. E*, **79** 032602 (2009)
- [13] APEL M., BOETTGER B., DIEPERS H.-J., AND STEINBACH I., *J. Cryst. Growth*, **237** 154 (2002)
- [14] LEWIS D. ET AL., *JOM-US*, **56** 34 (2004)
- [15] FOLCH R. and PLAPP M., *Phys. Rev. E*, **68** 010602(R) (2003)
- [16] FOLCH R. and PLAPP M., *Phys. Rev. E*, **72** 011602 (2005)
- [17] PERRUT M. ET AL., *Acta Mater.*, **58** 1761 (2010)
- [18] LEE J. H., LIU S. and TRIVEDI R., *Metall. Mat. Trans. A*, **36** 3111 (2005)
- [19] LIU S., LEE J.-H., ENLOW D. and TRIVEDI R., *Solidification Processes and Microstructures: A Symposium in Honor of Wilfried Kurz*, edited by RAPPAPAZ M., BECKER-MANN C. and TRIVEDI R. (TMS, Warrendale PA) 2004
- [20] RACEK R., LESOULT G. and TURPIN M., *J. Cryst. Growth*, **22** 210 (1974)
- [21] KOHLER F., GERMOND L., WAGNIÈRE J.-D. and RAPPAPAZ M., *Acta Mater.*, **57** 56 (2009)
- [22] JACKSON D. B. and GANTNER B., *Phys. Rev. E*, **64** 056230 (2001)
- [23] NI Y., HE L. H. and SONG J., *Surf. Sci.*, **553** 189 (2004)
- [24] MURATOV C. B., *Phys. Rev. Lett.*, **78** 3149 (1997)
- [25] GAREL T. and DONIACH S., *Phys. Rev. B*, **26** 325 (1982)
- [26] OUYANG Q. and SWINNEY H. L., *Nature*, **352** 610 (1991)
- [27] OUYANG Q., NOSZTICZIUS Z. and SWINNEY H. L., *J. Phys. Chem.*, **96** 6773 (1992)
- [28] GUNARATNE G. H., OUYANG Q. and SWINNEY H. L., *Phys. Rev. E*, **50** 2802 (1994)
- [29] HILALI M’F. ET AL., *Phys. Rev. E*, **51** 2046 (1995)